Revista Mexicana de Astronomía y Astrofísica, **33**, 157–164 (1997)

THE PROPER MOTIONS OF CONDENSATIONS IN A BOW SHOCK FLOW

A. C. Raga[1], J. Cantó[1], S. Curiel[1], A. Noriega-Crespo[2], and J. C. Raymond[3]

Received 1997 June 16; accepted 1997 August 18

RESUMEN

Desde hace más de una década, comparaciones entre perfiles de línea de alta resolución y modelos 3/2-D de choques a proa, han sido usadas para deducir las propiedades generales de los objetos Herbig-Haro (HH). En particular, los parámetros que han sido obtenidos son la velocidad del choque a proa, la dirección en la cual se está moviendo el objeto y el movimiento del medio ambiente sobre el cual está viajando el objeto. Este artículo presenta un análisis de cómo calcular estos parámetros con observaciones de movimientos propios de las condensaciones de un objeto HH. Derivamos expresiones sencillas para determinar los parámetros relevantes partiendo de mediciones de las componentes de los movimientos propios paralelas y perpendiculares al eje proyectado del flujo. Estas expresiones luego son aplicadas a los movimientos propios observados para HH 1, HH 32 y HH 34, para los cuales obtenemos los respectivos parámetros.

ABSTRACT

For over a decade, comparisons of high resolution line profiles with simple, 3/2-D bow shock models have been used to derive the general properties of Herbig-Haro (HH) objects. In particular, the parameters which have been derived are the bow shock velocity, the direction of motion of the object, and the motion of the environment into which the object is moving. This paper presents an analysis of how to derive these parameters from observations of proper motions of the condensations of a HH object. Simple expressions are derived for determining the relevant parameters from measurements of the components of the proper motion velocities along and perpendicular to the projected outflow axis. These prescriptions are then applied to the observed proper motions of HH 1, HH 32 and HH 34, for which we obtain the respective flow parameters.

Key words **HYDRODYNAMICS — ISM–JETS AND OUTFLOWS — PROPER MOTIONS**

1. INTRODUCTION

Hartmann & Raymond (1984) first used a 3/2-D bow shock model to reproduce different observational properties of Herbig-Haro (HH) objects. Such models have subsequently been used by a number of authors (Choe, Böhm, & Solf 1985; Raga & Böhm 1985, 1986; Hartigan, Raymond, & Hartmann 1987; Hartigan, Morse, & Raymond 1994; Henney 1996) to model the emission line profiles and emission maps of HH objects.

Of particular interest is the paper of Hartigan et al. (1987), in which simple, analytic expressions are derived for deducing the bow shock velocity and direction of motion (as well as the velocity of the environment ahead of the bow shock) from measurements of the maximum and minimum radial velocities detected in the emission line profiles. These analytic expressions have been most useful, and have been used to deduce parameters for many HH objects (see, e.g., Hartigan, Raymond, & Meaburn 1990).

It has been proposed by different authors (e.g., Raga & Böhm 1987; Raga et al. 1988; Blondin, Königl, & Fryxell 1989) that the unresolved condensations observed in the heads of objects like HH 1 and HH 34 are intensity enhancements in material that participates in the dynamics of a single, spatially re-

[1] Instituto de Astronomía, Universidad Nacional Autónoma de México.
[2] Infrared Processing and Analysis Center, USA.
[3] Harvard-Smithsonian Center for Astrophysics, USA.

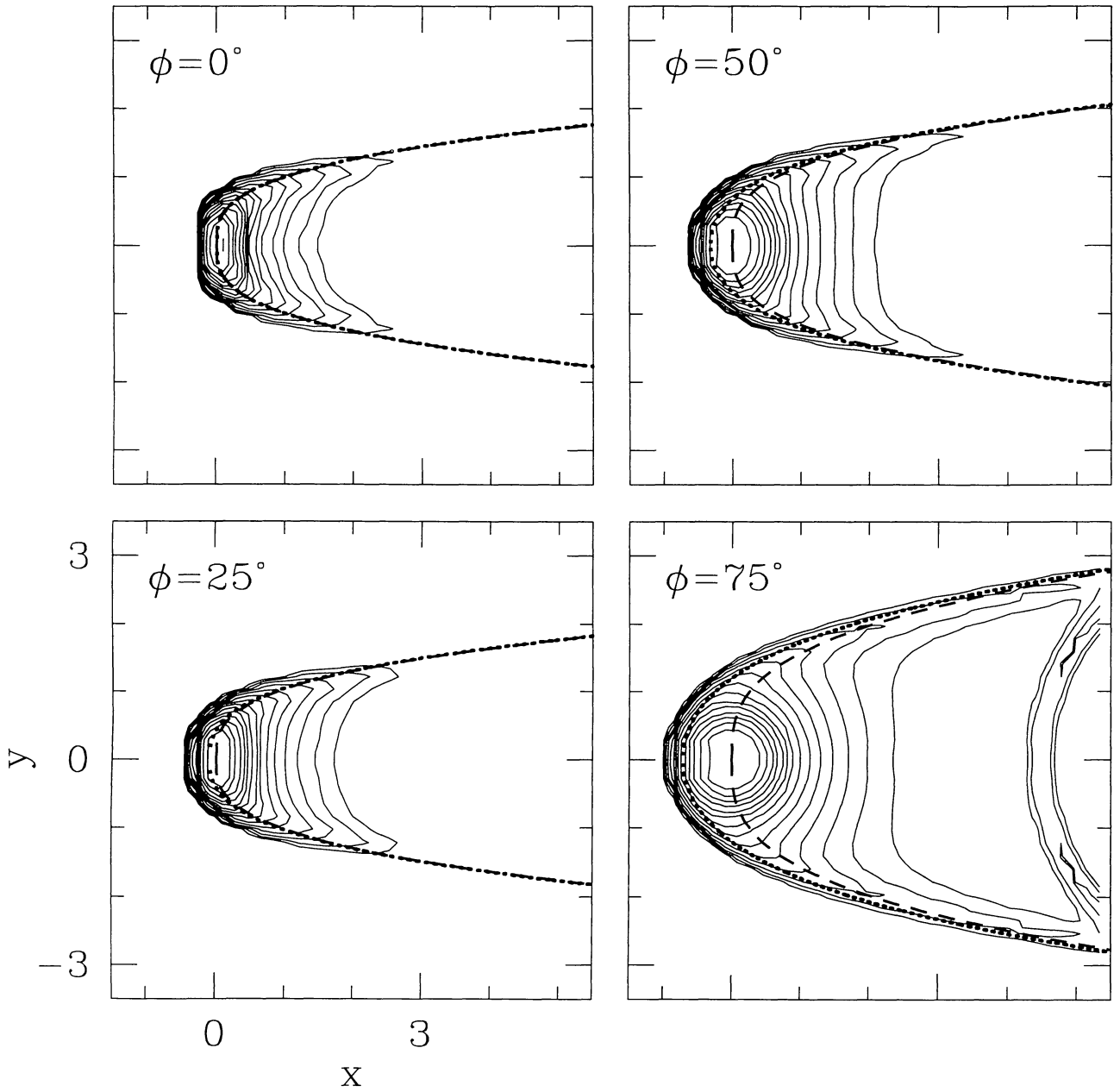

Fig. 1. Intensity maps predicted from the 3/2-D bow shock model described in the text. Two successive contours represent a factor of $2^{1/2}$ change in intensity. Maps are presented for angles $\phi = 0$, 25, 50 and 75° between the symmetry axis and the plane of the sky. A Gaussian seeing profile of FWHM=0.1 has been convolved with the predicted maps. The dotted lines show the edge of the projected bow shock, and the dashed lines indicate the position of the projected bow shock rim (see § 2).

solved bow shock. This picture appears to be confirmed by recent *Hubble Space Telescope (HST)* images of the heads of different HH objects (see, e.g., Reipurth & Heathcote 1997).

The present paper discusses the proper motions that would be observed for condensations that take part of the dynamics of a single bow shock. From a simple, 3/2-D bow shock model it is possible to obtain the motion of the post-shock gas projected onto the plane of the sky (as opposed to the radial velocities studied in previous papers). The general characteristics of the projection of a bow shock onto the plane of the sky are described in § 2. A detailed discussion of the motion of the gas is carried out in § 3. Finally, comparisons between the bow shock model and observations of three different HH

objects are used to derive different parameters of the observed flows in § 4.

2. THE PROJECTION OF A BOW SHOCK ONTO THE PLANE OF THE SKY

In 3/2-D bow shock models, it is assumed that the bow shock has a known shape, and that the emission is produced in a thin region behind the shock front. The material in this emitting region is assumed to have a velocity equal to the tangential component of the preshock flow.

In previous work, different parametrized shapes have been used for the bow shock. Raga & Böhm (1985) derived a parametrized, rational function which approximates the shape of a radiative bow shock formed in the flow around a solid sphere. Hartigan et al. (1987) used quadratic/quartic shapes for the bow shock. Finally, Henney (1996) studied bow shock shapes of arbitrary power law index (as well as non-axisymmetric shapes).

For presenting predictions of intensity maps, we choose a cubic, $z \propto r^3$ shape for the bow shock (where z is the distance measured along the symmetry axis, and r is the cylindrical radius). The rationale behind choosing this shape is that such a cubic solution is obtained for the momentum-conserving wings of a highly radiative bow shock flow, as shown by Wilkin (1996).

In order to obtain predictions of intensity maps, it is necessary to give a relation between the emission per unit area σ and the component v_n of the bow shock velocity normal to the local surface of the bow shock. For the sake of simplicity, we choose a $\sigma \propto {v_n}^3$ law, which is appropriate for the Hα intensity of shocks with velocities lower than $\sim$ 100 km s^{-1} (Raga & Kofman 1992).

With prescriptions $r = z^{1/3}$ (for the shape of the bow shock) and $\sigma = {v_n}^3$ (for the intensity per unit area), we have computed intensity maps for different angles ϕ between the symmetry axis and the plane of the sky (convolving the predicted emission with a Gaussian seeing profile of FWHM = 0.1). The results of this exercise (which is completely equivalent to the work of Raga 1986) are presented in Figure 1.

In Figure 1, we also show two curves: the edge of the projected bow shock (dotted line) and the projection of the rim of the bow shock onto the plane of the sky (dashed line). The physical meaning of this second curve is clarified in the schematic diagram of Figure 2, which is important for understanding the effect of the projection of the bow shock on local intensity maxima (condensations).

The points on the surface of the bow shock are determined by their position z along the symmetry axis, their cylindrical radius r (with z and r related by the parametrized function describing the bow shock shape), and their azimuthal angle θ (with

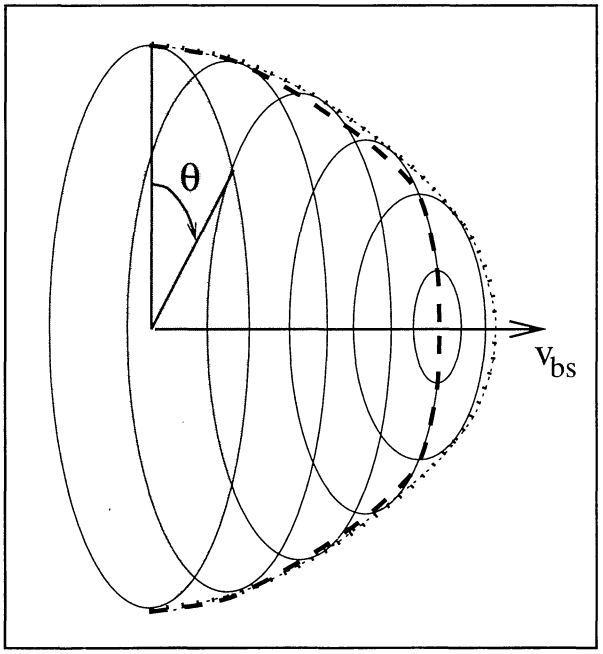

Fig. 2. Schematic diagram of the projection of a bow shock onto the plane of the sky. The bow shock moves at a velocity v_{bs}, which is directed at an angle ϕ into the plane of the diagram. The dotted line is the edge of the projected bow shock, and the dashed line represents the projection of the bow shock rim (the rim being defined as the line on the surface of the bow shock which has values of 0 or π for the azymuthal angle θ, which is shown in the diagram).

$\theta = 0$ and $\theta = \pi$ corresponding to directions parallel to the plane of the sky, see Fig. 2). The "rim" of the bow shock is the curve joining the points on the surface of the bow shock which have $\theta = 0$ or $\theta = \pi$ (Figure 2, dashed line). If the bow shock has a shape $r(z)$, it is then simple to show that the projection of the bow shock rim onto the (x, y) plane of the sky is given by

$$y(x) = r(x/\cos\phi)\,, \qquad (1)$$

where ϕ is the angle between the symmetry axis and the plane of the sky, and we have taken the origin of the coordinate system to coincide with the projection of the apex of the bow shock onto the plane of the sky.

Also shown in Figure 2 (dotted line) is the edge of the projected bow shock, i.e., the curve joining the points on the surface of the bow shock which are tangent to the line of sight. It is easy to show that for these points

$$\sin\theta = \frac{dr}{dz}\tan\phi\,. \qquad (2)$$

This equation follows from the fact that the scalar product of the unit vector parallel to the line of sight and the unit vector along the surface of the bow shock has to be equal to zero. Using eq. (2), and explicitly considering the spatial coincidence of the position along the line of sight with the surface, it can be shown that the curve describing the edge of the projected bow shock is given in a parametric way by

$$x = z \cos\phi \left[1 - \frac{r}{z}\frac{dr}{dz} \tan^2\phi\right] , \qquad (3)$$

$$y = r \left[1 - \left(\frac{dr}{dz}\right)^2 \tan^2\phi\right]^{1/2} , \qquad (4)$$

where z spans the range in which the condition

$$-\frac{1}{\tan\phi} \leq \frac{dr}{dz} \leq \frac{1}{\tan\phi} , \qquad (5)$$

is met. This condition follows from eq. (2).

The curves described by eq. (1) and by eqs. (3–5) are shown with a dashed and a dotted line (respectively), on the emission maps of Figure 1. For low values of the orientation angle ϕ, both lines coincide spatially. For large values of ϕ (i.e., approaching $\phi = 90°$), the two lines become clearly separate in the head of the bow shock.

From the emission contours (see Fig. 1), we see that the strongest intensities are obtained in the region close to these two lines. For example, for the $\phi = 0°$ map, the intensity is concentrated to a ridge surrounding the emitting region, which closely coincides with the two lines. For larger values of ϕ, the intensity ridge approximately follows the projection of the bow shock rim (see eq. 1).

This discussion is of interest for a qualitative analysis of a bow shock with local intensity maxima ("condensations"). If the bow shock has several intensity maxima distributed throughout its surface, it is clear that the maxima located close to the rim of the bow shock (defined by eq. 1) will be favoured by the projection, so that they will have stronger intensities in the projected emission maps. Because of this, condensations observed in HH bow shocks are probably located in regions close to the bow shock rim. As we will see in the following section, this result is important for the analysis of the proper motions of the condensations.

3. THE PROPER MOTIONS

Let us now consider the motion in the plane of the sky of the post-bow shock gas. It is straightforward to show that the component of the post-shock velocity parallel to the projected symmetry axis (the x-axis of Figure 1) is given by

$$v_{\parallel} = v_{bs} \left(\sin^2\alpha \cos\phi + \sin\alpha \cos\alpha \sin\theta \sin\phi\right) + v_e \cos\phi , \qquad (6)$$

and that the component perpendicular to the projected symmetry axis is given by

$$v_{\perp} = v_{bs} \sin\alpha \cos\alpha \cos\theta , \qquad (7)$$

where the tangent angle α is defined by $\tan\alpha = dr/dz$ (with $r(z)$ being the shape of the bow shock, see § 2), v_{bs} is the velocity of the bow shock relative to the local environment, and v_e is the velocity (assumed to be directed along the symmetry axis of the bow shock) of the (uniform) environment into which the bow shock is moving.

Let us first analyze the properties of $v_{\perp}$ for a bow shock of fixed orientation ϕ with respect to the plane of the sky. From eq. (7), we see that for a given α, the minimum and maximum velocities are obtained for $\theta = \pi$ and $\theta = 0$, respectively, and have values given by

$$v_{\perp,min}(\alpha) = -\frac{v_{bs}}{2} \sin 2\alpha , \qquad (8)$$

$$v_{\perp,max}(\alpha) = \frac{v_{bs}}{2} \sin 2\alpha . \qquad (9)$$

The maximum and the minimum over all of the values of the tangent angle α (which ranges from $\alpha = \pi/2$ to $\alpha = 0$) are equal to $\pm v_{bs}/2$, so that the total range of values of $v_{\perp}$ for the post-bow shock material is

$$\Delta v_{\perp} = v_{bs} . \qquad (10)$$

This prediction of the observed range of proper motion velocities perpendicular to the flow axis is very interesting, since it allows a simple way of obtaining the velocity of the bow shock (relative to the surrounding environment).

It is, of course, unclear whether or not the whole range of possible proper motions in a given object can be seen, since the proper motion measurements sample the flow field only at the current positions of bright condensations. Interestingly, the maximum and minimum values of $v_{\perp}$ (eqs. 8 and 9) are obtained along the projected bow shock rim (i.e., for $\theta = 0, \pi$, see also eq. 1), where the intensity maps have a strong ridge (see Fig. 1). Therefore, we expect to see the brighter condensations in the region that has the highest and lowest values of $v_{\perp}$, so that the observationally determined range of $v_{\perp}$ is likely to be close to the value predicted by eq. (10).

Let us now analyze the properties of $v_{\parallel}$. From eq. (6), we see that the minimum and maximum of $v_{\parallel}$ over all θ and α are given by

$$v_{\parallel,min} = v_{bs}\left(-\frac{\sin^2\phi}{2} + \cos\phi\,\sin^2\frac{\phi}{2}\right) + v_e\,\cos\phi \quad , \tag{11}$$

$$v_{\parallel,max} = v_{bs}\left(\frac{\sin^2\phi}{2} + \cos\phi\,\cos^2\frac{\phi}{2}\right) + v_e\,\cos\phi \quad , \tag{12}$$

which are attained for a value of the tangent angle $\alpha = \phi/2$ for $\theta = -\pi/2$, and $\alpha = (\pi - \phi)/2$ for $\theta = \pi/2$, respectively. We therefore, would predict that the total velocity range covered by the components parallel to the outflow axis of the observed proper motions would also be equal to the velocity v_{bs} of the bow shock relative to its surrounding environment (a result which is directly obtained by subtracting eq. 11 from eq. 12).

However, the minimum and maximum values of $v_\parallel$ (eqs. 11 and 12) are obtained for fluid parcels with azimuthal angles $\theta = \pm\pi/2$ (see above). As we have discussed in § 2, this central region of the projected bow shock has the lowest intensities (see the intensity maps of Fig. 1), so that we do not expect to observe bright condensations in this region.

If we want to obtain a prediction of the values of $v_\parallel$ for condensations with observed proper motions, it is more appropriate to consider the fluid parcels along the projected rim of the bow shock (i.e., with $\theta = 0,\ \pi$). From eq. (6) it directly follows that the minimum and maximum values of $v_\parallel$ for the parcels along the projected bow shock rim are given by

$$v_{rim,\parallel,min} = v_e\,\cos\phi \quad , \tag{13}$$

$$v_{rim,\parallel,max} = (v_{bs} + v_e)\,\cos\phi \quad . \tag{14}$$

From this discussion, we would then conclude that the expected range for the components along the flow axis of the observed proper motion velocities is

$$\Delta v_\parallel = v_{rim,\parallel,max} - v_{rim,\parallel,min} = v_{bs}\,\cos\phi \quad . \tag{15}$$

In this way, we have derived a quite powerful method for deriving the orientation angle ϕ, the velocity v_{bs} and the velocity of the surrounding environment v_e from observations of the proper motion velocities of the condensations of a bow shock. The procedure would be as follows:

i. The observed proper motion velocities are decomposed into components $v_\parallel$ along and $v_\perp$ across the projected axis of the outflow.

ii. From the observed total range of values of $v_\perp$ the value v_{bs} of the bow shock velocity relative to the surrounding environment (eq. 10) is directly obtained.

iii. From the observed total range of values of $v_\parallel$ and the value of v_{bs}, the orientation angle ϕ between the symmetry axis and the plane of the sky (eq. 15) can be determined.

iv. Finally, the minimum observed value of $v_\parallel$ can be taken and eq. (13) can be used to obtain an estimate of the velocity of the environment relative to the source of the HH objects.

In the following section, we apply this procedure to the observed proper motions of three HH objects.

Finally, to complete our discussion of the predicted maximum and minimum velocities for condensations with observed proper motions, let us consider the situation where the observed condensations are on the edge of the projected bow shock. This location is of course favoured by the increase in the emitting column density, which results in a limb brightening of the observed emission. To this effect, we substitute eq. (2) (which defines the points on the edge of the projected bow shock) into eqs. (6) and (7). The result is

$$v_{edge,\parallel} = v_{bs}\,\frac{\sin^2\alpha}{\cos\phi} + v_e\,\cos\phi \quad , \tag{16}$$

and

$$v_{edge,\perp} = v_{bs}\,\sin\alpha\,\cos\alpha\,\left(1 - \tan^2\alpha\,\tan^2\phi\right)^{1/2} \quad . \tag{17}$$

From eq. (16), the minimum parallel velocity (obtained for $\alpha = 0$) is

$$v_{edge,\parallel,min} = v_e\,\cos\phi \quad . \tag{18}$$

The maximum corresponds to the maximum value of α on the edge ($\alpha = \pi/2 - \phi$) given by the condition expressed by eq. (5). We then obtain

$$v_{edge,\parallel,max} = (v_{bs} + v_e)\,\cos\phi \quad . \tag{19}$$

Interestingly, these minimum and maximum velocities coincide with those found for the rim (eqs. 13 and 14), so that the expected range for the components along the flow axis is also the same (eq. 15).

For the perpendicular component eq. (17) can be differentiated to find the maximum and minimum values. The result is

$$v_{edge,\perp,max} = \frac{v_{bs}}{2}\,\cos\phi \quad , \tag{20}$$

$$v_{edge,\perp,min} = -\frac{v_{bs}}{2}\,\cos\phi \quad , \tag{21}$$

both reached at a tangent angle

$$\alpha = \arcsin\left(\frac{\cos\phi}{\sqrt{2}}\right) \quad , \tag{22}$$

which is always smaller than the maximum allowed value ($\alpha = \pi/2 - \phi$) given by eq. (5). The range of perpendicular velocities therefore, is

$$\Delta v_{edge,\perp} = v_{bs} \cos\phi \ , \qquad (23)$$

which is equal to the range covered by the parallel velocities.

4. AN ANALYSIS OF OBSERVED PROPER MOTIONS

In order to be able to carry out comparisons with observations, we need to find bow shock-like HH objects with several condensations with measured proper motion velocities. The only clear candidates appear to be the objects HH 32 A, HH 34 S and HH 1, which have successfully been modeled before as bow shocks, and for which appropriate proper motion measurements have been obtained. The other possible candidate is of course HH 2, which is very complex, so that an interpretation of this object in terms of a single bow shock model appears to be inappropriate (Indebetouw & Noriega-Crespo 1995; Moro-Martin et al. 1996).

The range of proper motion velocities perpendicular ($\Delta v_\perp$) and parallel ($\Delta v_\parallel$) to the projected outflow axis, as well as the minimum value ($v_{\parallel,min}$) of the velocity parallel to the axis obtained for these objects are listed in Table 1. This table also gives the bow shock velocity v_{bs} (relative to the pre-bow shock environment), the velocity v_e of the environment relative to the outflow source and the orientation angle ϕ (between the outflow axis and the plane of the sky) deduced using the method described in § 3.

Let us discuss in detail the results obtained for the three HH objects:

i) HH 32 A. Curiel et al. (1997) have measured proper motions for 5 subcondensations (A1–A5) of this object. We have taken the outflow axis to have a PA=287° direction (joining AS 353 A with HH 32 A). The measured values (see Table 1) result in a bow shock velocity $v_{bs} = 267$ km s^{-1}, an orientation angle $\phi = 72°$ and an environmental velocity $v_e = 49$ km s^{-1}. These values are completely consistent with the ones deduced from high resolution spectra by Solf, Böhm, & Raga (1986) and by Hartigan et al. (1987).

ii) HH 34 S. Eislöffel & Mundt (1992) have measured proper motions for 12 condensations of this bow shock. We have taken the outflow axis to have a PA=166°.5 direction (joining the well aligned knots of the HH 34 jet, which directly point towards HH 34 S). For obtaining the values shown in Table 1, we have ignored the proper motions of condensations D′, E and H, as these knots are not well defined in the images (which were used for the proper motion determinations), and they also show proper motions with anomalous moduli and/or directions. The value obtained for the bow shock velocity ($v_{bs} = 268$ km s^{-1}) is only somewhat higher than the $v_{bs} \approx 200$ km s^{-1} deduced from the total width of the [S II] 6717+6731 line profile presented by Heathcote & Reipurth (1992) or the Hα profile of Bührke, Mundt, & Ray (1988). On the other hand, somewhat lower values of v_{bs} are derived if one considers only the brighter region of the emission lines. The orientation angle of $\phi = 30°$ derived from the proper motions (see Table 1) is in excellent agreement with the (identical) value suggested by Heathcote & Reipurth (1992) and by Morse et al. (1992) (a somewhat lower, $\phi = 23°$ value having been suggested by Eislöffel & Mundt 1992). The $v_e = 188$ km s^{-1} value that we have derived for the velocity of the surrounding environment is also in excellent agreement with the 170 km s^{-1} value deduced by Morse et al. (1992).

iii) HH 1. Eislöffel, Mundt, & Böhm (1994) have measured proper motions for 12 condensations of this bow shock. For obtaining the values shown in Table 1, we have ignored the proper motion of conden-

TABLE 1

PROPER MOTIONS OF HH BOW SHOCKS AND DERIVED PARAMETERS

Object	HH 32 A	HH34 S	HH 1
Condensations	A1, A2, A3, A4, A5	A, B, C, C′, D, F, I, J	A, C, D, E, F, G, H, J, K, M, N
$\Delta v_\perp$ (km s^{-1})	267	268	147
$\Delta v_\parallel$ (km s^{-1})	82	232	275
$v_{\parallel,min}$ (km s^{-1})	15	163	106
v_{bs} (km s^{-1})	267	268	275
ϕ (°)	72	30	...
v_e (km s^{-1})	49	188	106

sation L, which has anomalously high proper motion, and is a not very well defined knot. There is a problem in defining the axis of the outflow. If we draw a line joining the source of the outflow (VLA 1: Pravdo et al. 1985) with HH 1 F, we see that all the proper motion vectors point southwards of this line. We have therefore, taken the direction PA= 317°.5 (parallel to the direction of the proper motion of HH 1 F) as the outflow axis. The values obtained for $\Delta v_\perp$ and $\Delta v_\parallel$ are obviously somewhat problematic, as $\Delta v_\perp < \Delta v_\parallel$, which is not possible if the bow shock flow field is well sampled by the condensations (see eqs. 10 and 15, and the discussion of § 3). Therefore, the condensations of HH 1 must be located in positions that do not give us the total range of values of $v_\perp$ for the post-bow shock flow. All that we can then do is to take the value of $\Delta v_\parallel$ as an estimate of the bow shock velocity, which gives us the $v_{bs} = 275$ km s^{-1} value listed in Table 1. This estimate should be approximately correct, given the fact that the HH 1/2 outflow axis lies very close to the plane of the sky (Böhm & Solf 1985). However, we find this value to be considerably higher than the 148 km s^{-1} value deduced from the Hα line profile of HH 1 F by Hartigan et al. (1987), and also higher than the 185 km s^{-1} value deduced by Raga et al. (1988) from a comparison with an Hα position-velocity diagram. The velocity for the environment $v_e = 106$ km s^{-1} listed in Table 1 has been computed from eq. (13), setting $\phi \approx 0$.

Let us summarize the above discussion. From the three objects that we have analyzed, for HH 32 we definitely obtain the best agreement between the parameters derived from our analysis of proper motions and the parameters that were previously derived from analyses of high resolution line profiles. For HH 34 we obtain a very good agreement with previous results for the value of the orientation angle of the flow axis. On the other hand, we obtain a value for the bow shock velocity that is $\sim$ 30–50% higher than the ones derived from high resolution line profiles of this object. Finally, for HH 1 we find clear difficulties in applying our method for analyzing the proper motion velocities. If we attempt to obtain an estimate for the bow shock velocity from the observed proper motions, we obtain a value that is $\sim$ 50% higher than the velocity derived from the emission line profiles of this object.

5. CONCLUSIONS

We have presented a simple, analytic formalism for analyzing the proper motions of bow shock-like HH objects. We derive very simple prescriptions for obtaining the bow shock velocity (with respect to the surrounding environment), the orientation angle of the flow axis (with respect to the plane of the sky), and the motion away from the source of the environment into which the bow shock is moving. These prescriptions are analogous to the ones derived by Hartigan et al. (1987) for analyzing the radial velocities of a bow shock flow.

We have then applied this analysis to the proper motions which have been obtained by other authors for HH 32 A, HH 34 S and HH 1. While for HH 34 S and HH 1 we obtain only a partial success at reproducing the previously determined parameters for these objects, for HH 32 A we obtain an almost perfect agreement. This is not completely surprising, since the proper motions for the subcondensations of HH 32 A (Curiel et al. 1997) have been determined from a combination of very high spatial resolution images (obtained with the *Hubble Space Telescope* and with the Canada-France-Hawaii Telescope), probably resulting in a higher accuracy.

From this experience, we expect our method for analyzing proper motions of bow shocks to be very useful in the near future, when detailed proper motion measurements based solely on *HST* images will become available.

A particularly interesting problem is that our method does not work so well for HH 1, for which the proper motions have been measured with considerable accuracy (see Herbig & Jones 1981; Raga, Barnes, & Mateo 1990; Eislöffel et al. 1994). If these proper motions were not so accurate, it could be argued that if the high proper motion measured for condensation HH 1 F is eliminated, the discrepancy between the measured proper motion components along and across the axis would disappear (see § 4 item *iii)*. Furthermore, HH 1F shows quite strong H_2 emission (Davis, Eislöffel, & Ray 1994; Noriega-Crespo & Garnavich 1994), with a proper motion which agrees with the one measured optically (Noriega-Crespo et al. 1997). From this we would conclude that the proper motion measured for HH 1 F is indeed correct, and should not be eliminated for carrying out the comparison with our model.

Interestingly, if we look at the proper motions measured in the past for HH 32 (Herbig & Jones 1983) we see an effect similar to the one that we find for HH 1, namely that the proper motion component along the axis of the outflow has a dispersion which is considerably larger than the one of the component perpendicular to the outflow axis. Only in the newer, higher spatial resolution observations of Curiel et al. (1997) we see a breakup of condensation HH 32 A into several subcondensations, which have a large velocity dispersion perpendicular to the outflow axis. We can only speculate whether a similar effect might occur when proper motions are measured for the subcondensations of HH 1 F seen in *HST* images of this object (which are available electronically from the STScI home page, but as far as we are aware still not published).

Finally, we should note again that the method de-

scribed in this paper is based on the assumption that the condensations in a HH bow shock strictly follow the kinematics of a smooth, unperturbed, quasi-1D bow shock. As there has been no detailed study of the proper motions of condensations in numerical simulations of the head of a radiative jet, it is at this time unclear to what extent this assumption might be incorrect.

AR, JC and SC acknowledge support from CONACYT, DGAPA (UNAM) and the UNAM/Cray research program. ANC's research is supported by NASA Long Term Astrophysics Program through JPL under contract with the California Institute of Technology. We would like to thank K. H. Böhm (the referee) for very helpful comments.

REFERENCES

Blondin, J. M., Königl, A., & Fryxell, B. A. 1989, ApJ, 337, L37
Böhm, K. H., & Solf, J. 1985, ApJ, 294, 533
Bührke, T., Mundt, R., & Ray, T. P. 1988, A&A, 200, 99
Choe, S. U., Böhm, K. H., & Solf, J. 1985, ApJ, 288, 338
Curiel, S., Raga, A. C., Raymond, J. C., Noriega-Crespo, A., & Cantó, J. 1997, AJ, in press
Davis, C. J., Eislöffel, J., & Ray, T. P. 1994, ApJ, 426, L93
Eislöffel, J., & Mundt, R. 1992, A&A, 263, 292
Eislöffel, J., Mundt, R., & Böhm, K. H. 1994, AJ, 108, 1042
Hartigan, P., Morse, J., & Raymond, J. C., 1994, ApJ, 436, 125
Hartigan, P., Raymond, J. C., & Hartmann, L. 1987, ApJ, 316, 323
Hartigan, P., Raymond, J. C., & Meaburn, J. 1990, ApJ, 362, 624
Hartmann, L., & Raymond, J. C. 1984, ApJ, 276, 560
Heathcote, S., & Reipurth, B. 1992, AJ, 104, 2193
Henney, W. J. 1996, RevMexAA, 32, 1
Herbig, G. H., & Jones, B. F. 1981, AJ, 86, 1232
_____. 1983, AJ, 88, 1040
Indebetouw, R., & Noriega-Crespo, A. 1995, AJ, 109, 752
Moro-Martin, A., Noriega-Crespo, A ., Böhm, K.-H., & Raga, A. C. 1996, RevMexAA, 32, 75
Morse, J. A., Hartigan, P., Cecil, G., Raymond, J. C., & Heathcote, S. 1992, ApJ, 399, 231
Noriega-Crespo, A., & Garnavich, P. M. 1994, RevMexAA, 28, 173
Noriega-Crespo, A., Garnavich, P. M., Curiel, S., Raga, A. C., & Ayala S. 1997, ApJ, 486, L55
Pravdo, S. H., Rodríguez, L. F., Curiel, S., Cantó, J., Torrelles, J. M., Becker, R. H., & Sellgren, K. 1985, ApJ, 293, L35
Raga, A. C. 1986, AJ, 92, 637
Raga, A. C., & Böhm, K. H. 1985, ApJS, 58, 201
_____. 1986, ApJ, 308, 829
_____. 1987, ApJ, 323, 193
Raga, A. C, & Kofman, L. 1992, ApJ, 386, 222
Raga, A. C., Barnes, P. J., & Mateo, M. 1990, AJ, 99, 1912
Raga, A. C., Mateo, M., Böhm, K. H., & Solf, J. 1988, AJ, 95, 1783
Reipurth, B., & Heathcote, S. 1997, in Herbig-Haro Objects and the Birth of Low Mass Stars, ed. B. Reipurth & C. Bertout (Dordrecht: Reidel), 3
Solf, J., Böhm, K. H., & Raga, A. C. 1986, ApJ, 305, 795
Wilkin, F. 1996, ApJ, 459, L31

Jorge Cantó, Salvador Curiel, and Alejandro C. Raga: Instituto de Astronomía, UNAM, Apartado Postal 70-264, 04510 México, D.F., México. (raga@astroscu.unam.mx).
Alberto Noriega-Crespo: Infrared Processing and Analysis Center, Pasadena, CA 91125, USA
J. C. Raymond: Harvard-Smithsonian Center for Astrophysics, 60 Garden St., Cambridge, MA 02138, USA